nuclear fusion
IAEA

PAPER

Excitation of elliptical and toroidal Alfvén eigenmodes by ^{3}He-ions of the MeV-energy range in hydrogen-rich JET plasmas

To cite this article: V.G. Kiptily *et al* 2020 *Nucl. Fusion* **60** 112003

View the article online for updates and enhancements.

IOP ebooks™

Bringing together innovative digital publishing with leading authors from the global scientific community.

Start exploring the collection–download the first chapter of every title for free.

This content was downloaded from IP address 194.81.223.66 on 05/11/2020 at 13:40

IOP Publishing | International Atomic Energy Agency Nuclear Fusion

Nucl. Fusion **60** (2020) 112003 (9pp) https://doi.org/10.1088/1741-4326/ab79cb

Excitation of elliptical and toroidal Alfvén eigenmodes by ^{3}He-ions of the MeV-energy range in hydrogen-rich JET plasmas

V.G. Kiptily[1,a], Ye. Kazakov[2], M. Fitzgerald[1], M. Nocente[3,4], M. Iliasova[5], E. Khilkevich[5], M.J. Mantsinen[6,7], M.F.F. Nave[8], J. Ongena[2], S.E. Sharapov[1], A.E. Shevelev[5], Ž. Štancar[9], G. Szepesi[1], D.M.A. Taylor[1], Yu.V. Yakovenko[10] and JET Contributors[a]

[1] Culham Centre for Fusion Energy of UKAEA, Culham Science Centre, Abingdon, United Kingdom of Great Britain and Northern Ireland
[2] LPP-ERM/KMS, Association EUROFUSION-Belgian State, TEC partner, Brussels, Belgium
[3] Dipartimento di Fisica 'G. Occhialini', Università di Milano-Bicocca, Milano, Italy
[4] Institute for Plasma Science and Technology, National Research Council, Milano, Italy
[5] Ioffe Institute of the Russian Academy of Sciences, St Petersburg 194021, Russian Federation
[6] Barcelona Supercomputing Centre, Barcelona, Spain
[7] ICREA, Pg. Liuis Companys 23, 08010, Barcelona, Spain
[8] Instituto de Plasmas e Fusão Nuclear, Instituto Superior Técnico, Universidade de Lisboa, Portugal
[9] Slovenian Fusion Association, Jozef Stefan Institute, Jamova 39, SI-1000, Ljubljana, Slovenia
[10] Kyiv Institute for Nuclear Research, Prospekt Nauky 47, Kyiv 03680, Ukraine

E-mail: vasili.kiptily@ukaea.uk

Received 12 December 2019, revised 4 February 2020
Accepted for publication 25 February 2020
Published 25 August 2020

Abstract

Elliptical (EAE) and toroidal Alfvén eigenmode (TAE) instabilities have been observed in hydrogen-rich JET discharges of the *D*-(^{3}He)-*H* ion cyclotron resonance heating (ICRH) scenario, which is characterized by strong absorption of radio frequency waves at very low concentrations of the resonant ^{3}He-ions. In the experiments, core localized TAEs with a frequency $f_{\mathrm{TAE}} \approx 280$ kHz with mode numbers $n = 3$, 4, 5 and 6 were detected. Following the phase with TAE excitation, EAE modes at higher frequencies $f_{\mathrm{EAE}} \approx 550$–580 kHz with mode numbers $n = 1$, 3, 5 were seen. These high frequency modes indicate that a MeV range population of trapped energetic ions was present in the plasma. The experimental evidence of existence of the MeV-energy ^{3}He-ions able to excite the AEs is provided by neutron and gamma-ray diagnostics as well as fast ion loss measurements. The ICRH modelling code calculations confirm the acceleration of ^{3}He-ions to MeV energies. The magnetohydrodynamic (MHD) analysis results are consistent with the experimental data showing that the MeV ^{3}He ions satisfy to resonant conditions interacting with TAE and EAE modes. This experiment demonstrates the efficient plasma heating mimicking the conditions representative for the ITER plasmas and contribute to the understanding of fast-ion interaction with MHD wave modes.

Keywords: tokamak, ICRF heating, diagnostics, MHD

(Some figures may appear in colour only in the online journal)

[a] See Klinger et al 2019 (https://doi.org/10.1088/1741-4326/ab03a7) for the JET team.

 © 2020 IAEA, Vienna Printed in the UK

1. Introduction

Ion cyclotron range of frequencies (ICRF) heating is a powerful instrument to obtain bulk ion and/or electron heating in a variety of plasmas. In this work we used an extremely efficient ICRF absorption scheme, which relies on the presence of three ion species in the plasma, so-called 'three-ion scenario' [1]. It is very effective technique for fast-ion generation that has been demonstrated on Alcator C-Mod, AUG and JET [2, 3]. In our case, it is *D*-(^{3}He)-*H* three ion ICRH scenario. Hydrogen and deuterium are target plasma species with different fundamental ion-cyclotron frequencies ω_{ci} and a small amount of ^{3}He-ions is minority of resonant ions as its charge-to-mass ratio satisfies the relation $(Z/A)_2 < (Z/A)_3 < (Z/A)_1$, i.e. 1/2 < 2/3 < 1/1. In this scenario the left-hand polarized component of the RF electric field E_+, which is rotating with ions, is strongly enhanced in the vicinity of the mode conversion (MC) layer and in this region an intense wave damping occurs by ^{3}He-ions that satisfies the resonance condition $\omega \approx \omega_{ci} + k_{\|} v_{\|}$.

The elliptical and toroidal Alfvén Eigenmode (as apt EAE and TAE) instabilities we observed in the hydrogen-rich discharge #91304 with up to 4.5 MW of ICRH power (P_{ICRH}) applied at $f = \omega/(2\pi) \approx 32.5$ MHz at toroidal field in the plasma centre $B_{\mathrm{T}}(0) = 3.1$ T and the central plasma density $n_{e0} \approx 4 \times 10^{19}$ m^{-3}. The *H*-ion cyclotron resonance lays at $R_{\mathrm{IC}} \approx 4.3$ m is outside the JET vessel. The *D*-ion cyclotron resonance is placed at $R_{\mathrm{IC}} \approx 2.15$ m, while the MC layer is in the plasma centre $R_0 = 2.96$ m (figure 1). It is important to emphasise that concentration of ^{3}He-ions was very low (X[^{3}He] < 1%) in this discharge.

An illustration of the time evolution of several plasma parameters during this JET pulse is found in figure 2. The ratio $n_{\mathrm{H}}/(n_{\mathrm{H}} + n_{\mathrm{D}})$ measured at the plasma edge varied during the heating period from ~90% to ~70%. One can see that from the beginning of the ICRF heating the plasma energy efficiently grows up with a rate $\Delta W_{\mathrm{P}}/\Delta P_{\mathrm{ICRH}} \approx 0.18$ MJ/MW. Since the ICRH power was coupled with asymmetric $+\pi/2$ antenna phasing, launching waves predominantly in the direction of the plasma current, a population of energetic ^{3}He ions was generated in the plasma, resulting in the long sawtooth (ST) periods ('monster sawtooth'). In the monster sawtooth period $t \approx 10$–10.4 s the core localized TAEs with mode numbers $n = 3, 4, 5, 6$ at a frequency $f_{\mathrm{TAE}} \approx 280$ kHz were observed. Following the phase with TAE excitation, strong EAE modes at higher frequencies $f_{\mathrm{EAE}} \approx 550$–580 kHz with mode numbers $n = 1, 3, 5$ were seen in period $t \approx 10.6$–10.8 s (figure 3). These high frequency modes indicate that a MeV range population of trapped energetic ions is present in the plasma interacting with the modes. Note that although we will show that MeV range ions are necessary for the observed modes, a full stability calculation with drive and damping mechanisms must be conducted in order to determine if they are sufficient, and indeed, why TAEs are not observed when EAEs are in this case.

The experimental evidence of the existence of the confined MeV-energy ^{3}He-ions able to excite the AEs and their loss due to the instabilities obtained with neutron and gamma-ray diagnostics as well as escaped fast ion measurements is provided in the next chapter. The MHD analysis results are presented in chapter 3. The paper is completed with a summary and conclusions.

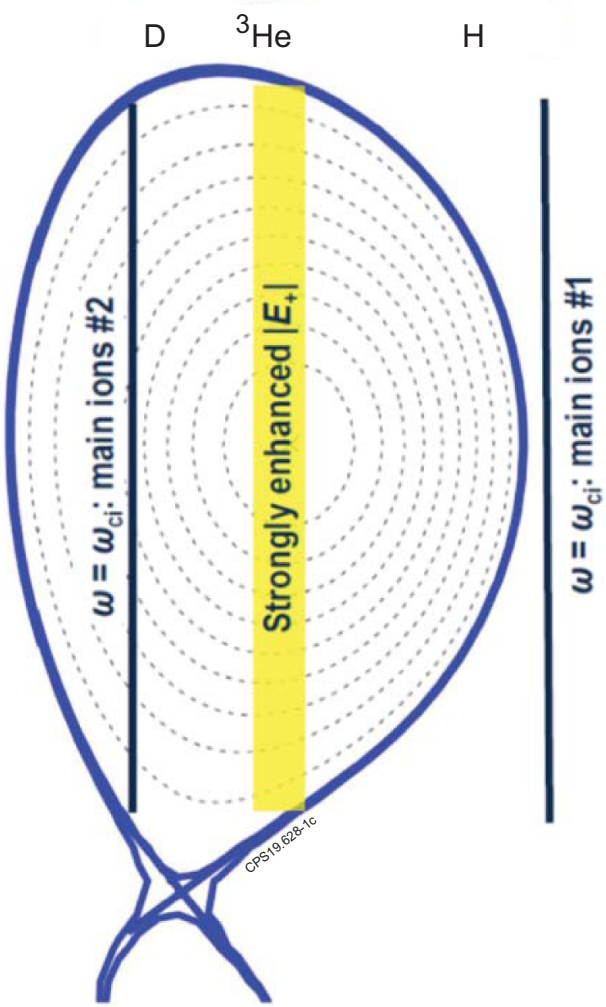

Figure 1. Resonant layers in the 'three-ion' scenario experiment with the central toroidal magnetic field $B_{\mathrm{T}}(0) = 3.1$ T and $f = 32.5$ MHz.

2. Observation of the confined and lost MeV-energy ^{3}He-ions

JET is equipped with an excellent set of diagnostics to study confined and escaped fast ions. Gamma-ray spectrometry [4] routinely used for the fast-ion studies in JET is based on measurements of gamma-rays, which are born as a result of nuclear reactions between confined fast ions and the main plasma intrinsic low-Z impurities in JET (*Be* and some *C*). This diagnostic provides information on the fast-ion tail in the MeV-energy range. In these experiments, gamma-ray energy spectra were recorded by a collimated $LaBr_3$ scintillation detector with a vertical line-of-sight through the plasma centre [5]. The DD neutron rate is monitored with a calibrated set of fission chambers [6]. The fast ion lost detector (FILD) [7]

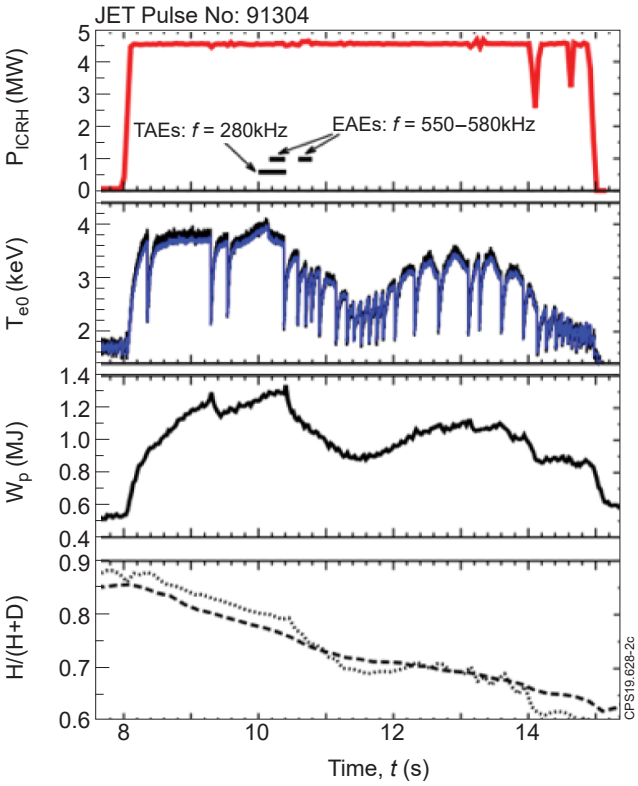

Figure 2. Waveforms and signals of some key quantities of the 'three-ion' scenario discharge #91304 at $B_T(0)$ =3.1 T, I_P =1.8 MA with $P_{ICRH} \approx 4.5$ MW at $f_{ICRH} \approx 32.5$ MHz; T_{e0}—the central electron temperature, W_P—the plasma energy and $H/(H+D)$—a relative concentration of hydrogen measured in the divertor plasma (dotted line) and from the gas beneath the divertor (dash line).

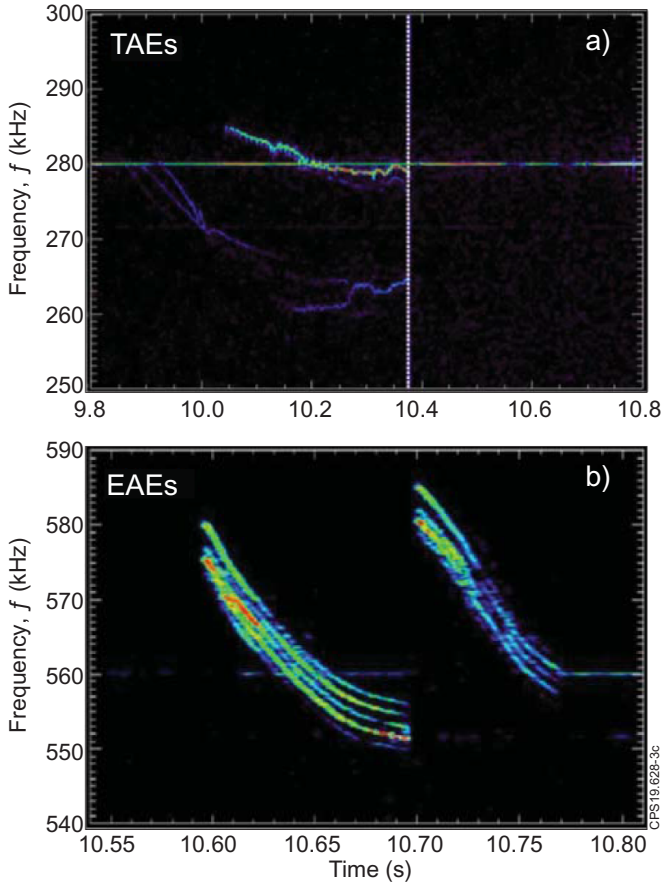

Figure 3. Magnetic spectrograms of TAEs (*a*) and EAEs (*b*) exited during the period t = 9.8–10.8 s in the discussed JET discharge.

allows detection of lost ions at a single position outside the plasma, and provides information on the lost ion pitch angle, $\theta = \cos^{-1}(v_{\|}/v)$, between 35° and 85° (~5% resolution) and its gyro-radius ρ_{gyr} between 3 and 14 cm (~15% resolution) with a time resolution of 2 ms. The grid (ρ_{gyr}, θ) on the scintillator plate calculated using EFIT equilibrium. FILD is in vessel ~28 cm below the mid-plane of the JET torus. The light emitted by the scintillator due to fast ion strikes is transported through a guide tube and a coherent fibre bundle to a charge-coupled device (CCD) and a photomultiplier (PMT) array.

The analysis of gamma-ray spectra recorded during the period of TAEs and EAEs excitation shows that identified gamma-ray peaks are related to the ^{3}He nuclear reactions: ^{9}Be(^{3}He,$n\gamma$)^{11}C and ^{9}Be(^{3}He,$p\gamma$)^{11}B. These reactions become intensive and can be detected with the diagnostics in JET, if energies of ^{3}He-ions E_{3He} > 0.9 MeV. The analysis of the gamma-ray spectra has been made with a special deconvolution code DeGaSum [8] developed for fusion plasma studies. Response functions of the spectrometer were calculated with Monte-Carlo code MCNP [9], using the detector line-of-sight model. Figure 4 shows experimental spectrum, the identified gamma-ray lines and the re-convoluted spectrum demonstrating the quality of the analysis. Gamma-rays with energies E_γ = 2.13, 4.44 and 7.29 MeV are related to transitions in the excited nucleus $^{11}B^*$ and E_γ = 2.00, 4.32, 6.34, 6.48 and 6.91 MeV in the ^{11}C*. Using the obtained intensities of gamma-ray lines and known partial cross-sections of the nuclear reactions we reconstructed energy distribution functions of ^{3}He-ions in the Maxwellian approximation (figure 5(*a*)). The effective temperature of ions in the TAEs period of the discharge (8.0–10.3 s) is T_{3He} ~ 1 MeV and it is ~0.7 MeV in the period of the EAE appearance (10.3–14 s). So, during the excitation TAEs and EAEs the ^{3}He-ions are extremely fast having energy in the MeV-range, which make them potentially responsible for triggering the modes. It should be noted that we did not find gamma-ray lines related to the ^{9}Be(D,$p\gamma$)^{10}Be and ^{9}Be(D,$n\gamma$)^{10}B reactions in the recorded spectra. These gammas could appear when the D-ion energies are in the range E_D > 0.5 MeV.

The calculations of the ^{3}He-ion distribution with the ICRF modelling code PION [10] have been made. The ^{3}He-ion tail temperatures as a function of the square root of normalized poloidal flux is presented in figure 5(*b*). It is seen that the ^{3}He-ion tail temperature in the plasma centre is at ~1 MeV and this is in the good agreement with the central line-integrated gamma-ray spectra measurements. There is no indication that ICRF power absorbed by D-ions as the fundamental ion-cyclotron resonance is located at the high-field side plasma edge (figure 1).

In addition, we established that the neutron rate in this ICRH-only hydrogen-reach plasma discharge is anomalously

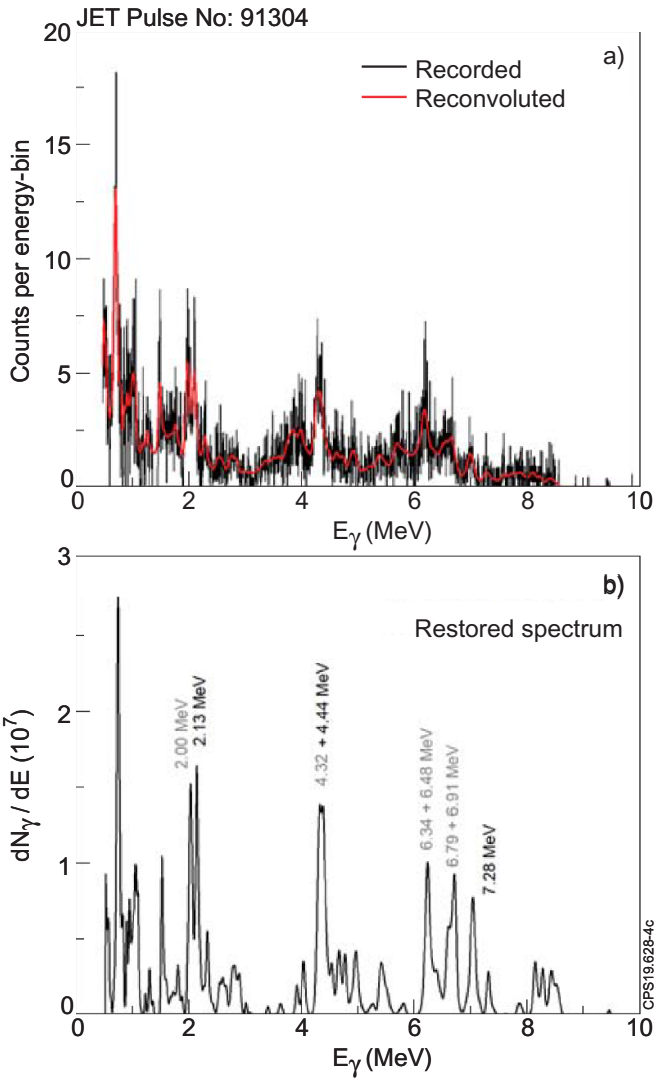

Figure 4. Results of gamma-ray spectrum analysis: (*a*)—spectrum recorded during $t = 8.0$–10.3 s (black); (*b*)—gamma-ray spectrum deconvoluted with DeGaSum [8]; gamma-ray energies related to the reactions ^{9}Be(^{3}He,$n\gamma$)^{11}C (grey) and ^{9}Be(^{3}He,$p\gamma$)^{11}B (black). The re-convoluted spectrum is shown in the upper (*a*) in red.

high (figure 6). It is seen that during the both first and second monster sawteeth, during very efficient plasma heating, neutron rate grows dramatically. To compare the thermal DD neutron rate, which is expected, with experimental one the TRANSP calculations were made. Since the ratio $n_D/(n_H + n_D)$ was growing in the sawteeth period, the calculations were done for 6 periods averaged ratios in each time-bin. Figure 7 shows comparison of the TRANSP calculations, including the uncertainty band related to the deuterium concentration variation, and measured neutron rate. One can see that measured rate up to ~4 times higher than expected with $T_i = T_e$. One of the possible sources of the anomalous rate increase could be a knock-on effect [11]. The gamma-ray measurements confirm the MeV-energy tail of ^{3}He-ions accelerated due to ICRH, hence the Coulomb and nuclear d-^{3}He scattering could generate supra-thermal deuteron distribution thereby greatly enhancing D(d,n)^{3}He reaction rate. Also, ^{3}He-ions with $E_{3He} > 0.9$ MeV can give rise additional neutrons due to the nuclear reaction ^{9}Be(^{3}He,n)^{11}C. Indeed, neutron energies up to 10 MeV have been detected with high-resolution neutron spectrometer TOFOR during fast-ion studies with ^{3}He- minority ICRF heating on JET [12]. Depending on Be concentration, a contribution up to ~10%–50% to the total neutron yield from the ^{9}Be(^{3}He,n)^{11}C reaction was found.

In figure 6 one can see sharp transient spikes of the neutron rate at time of the monster sawtooth crashes. We can suggest that 10%–20% of neutron rate increase could be caused by D-ion acceleration by the sawtooth reconnection electric field. Obtaining this estimate, we assume that the crashes result from a Sweet-Parker type reconnection and use extended Ohm's law involving the electron inertia [13] and pressure [14]. The change of the particle kinetic energy, W, was evaluated using results [15, 16]. For D-ions, we obtain that $\Delta W / W \sim 0.03$. In the keV-range the cross-section of the D(d,n)^{3}He reaction [17] has a steep slope and the sawtooth reconnection W changes can lead to the reactivity increase ~20% and it could account for the observed effect. It should be noted that only a fraction of ions can pass through the reconnection layer (because the reconnection is asymmetric), hence the expected reactivity growth is smaller. Also, there is an additional way to generate extra neutrons in the sawtooth crashes. It could be caused by a massive escape of the MeV ^{3}He-ions due to the crash. Since the modern JET has beryllium wall (so named the JET ITER-like wall), the ^{9}Be(^{3}He,n)^{11}C reactions give rise neutrons [12].

The fast ion losses detected with FILD indicate that escaped ^{3}He-ions are very energetic laying in the MeV-energy range. Indeed, the footprint of losses shown in figure 8(*a*) demonstrates that ions lost in the period of TAEs $t = 9.94$–10.34 s have the gyro-radius in the range $\rho_{gyr} > 10$ cm with pitch-angles $\theta \approx 60°$–$66°$. The energy of ions is related to the gyro-radius as

$$E_i = \left[\frac{\rho_{gyr}\,(\mathrm{cm})\,B_{FILD}\,(T)}{14.45}\right]^2 \frac{Z_i^2}{A_i}, \qquad (1)$$

where B_{FILD} is magnetic field at the location of the FILD scintillator plate, which in the presented case, ≈2.38 T. Therefore, escaping ^{3}He-ions have energies $E_i > 3.6$ MeV in the TAEs period. However, losses due to the monster sawtooth crash (figure 8(*b*)) at t ≈ 10.4 s aligned along the $\theta \approx 68°$ are related to ^{3}He-ions in the broader energy range $E_i > 1.8$ MeV ($\rho_{gyr} > 7$ cm). It is quite difficult to separate the CCD footprint loss contributions related TAEs, ST and EAEs because of a finite $\Delta\rho_{gyr}$ and $\Delta\theta$ resolution and a rather weak light emissivity of FILD in this discharge. However, we obtained a reasonable quality footprint integrating the scintillator light emission in the whole interested period $t = 10$–10.8 s (figure 9(*a*)). Selecting the large gyro-radius area related to high-energy ions, as shown in figure 9(*a*) ($\rho_{gyr} \approx 11$–13.5 cm, $\theta \approx 60°$–$66°$), we produced a waveform of losses, which is presented in figure 9(*b*). This waveform demonstrates increase of the loss rate during TAEs ($t \approx 10$–10.4 s) with a sawtooth crash peak at ≈10.4 s. Also, two strong peaks of losses related to EAEs excited in the periods $t \approx 10.6$–10.7 s and $t \approx 10.7$–10.8 s.

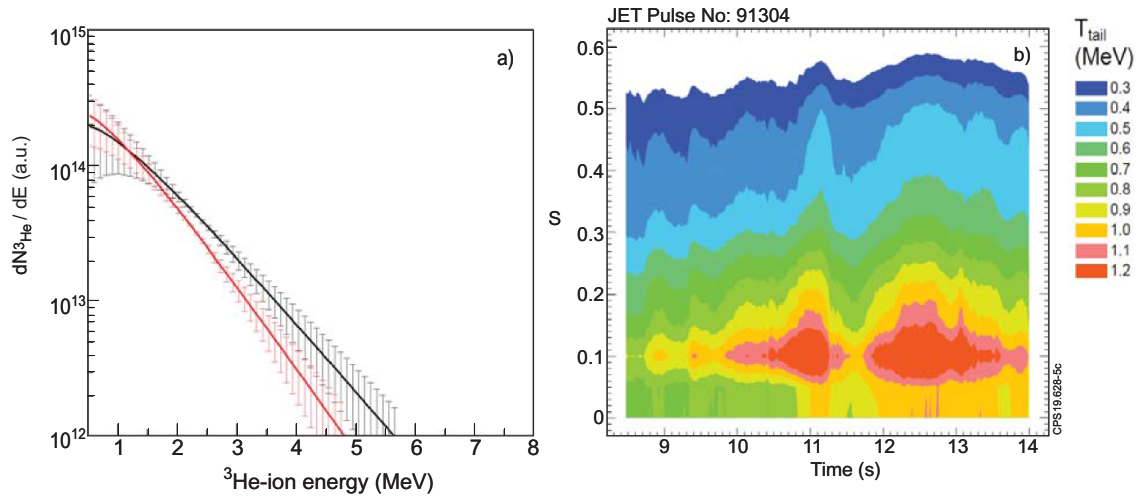

Figure 5. (*a*)—Energy distributions of ^{3}He-ions obtained from gamma-ray spectra recorded in the periods of the discharge 8.0–10.3 s (black line) and 10.3–14 s (red line); (*b*)—the PION calculation results the radial dependence of the ^{3}He-ion tail temperature as a function of the square root of normalized poloidal flux *s*.

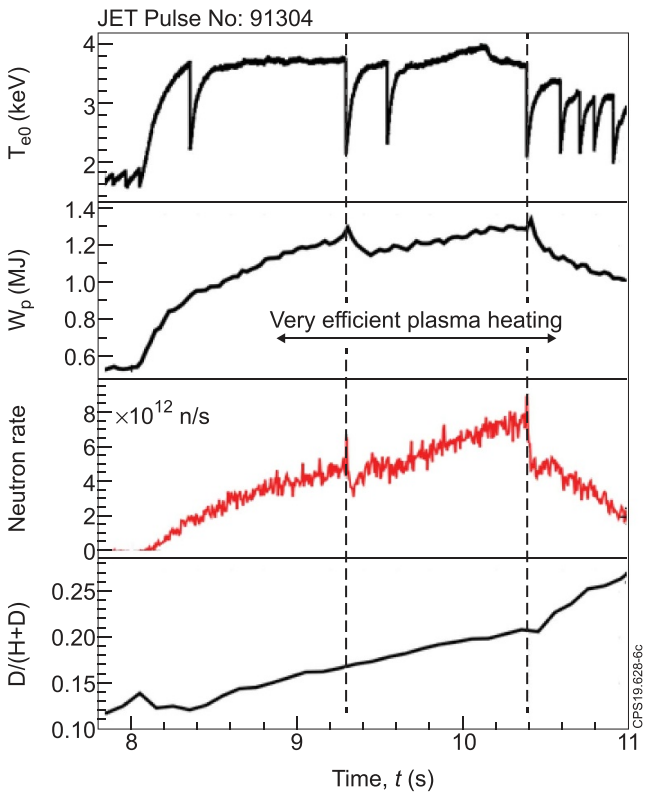

Figure 6. Waveforms and signals of the discharge discussed in the paper: T_{e0}—central electron temperature; W_p—the plasma energy; neutron rate and $D/(H+D)$—a relative concentration of deuterium.

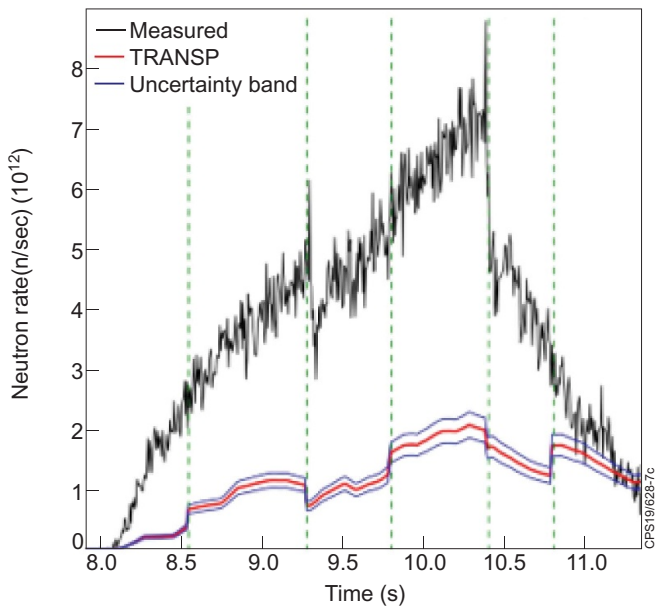

Figure 7. Neutron rate measured during the discharge and calculated one by TRANSP in six time slots with D-ion densities averaged over the time slot and uncertainty band.

Using the data presented in figure 9(*a*), we obtained a pitch-angle distribution of lost ions with $\rho_{gyr} = 13$ cm related to energies $E_i \approx 6$ MeV of ^{3}He-ions (figure 10). One can see that maximum of the distribution is at $\theta \approx 64°$. It is important to note that the major radius at the ion bounce reflection and the pitch-angle θ of the grid are related by

$$R(\theta) = R_{FILD}\sin^2\theta, \tag{2}$$

where $R_{FILD} = 3.825$ m is radial position of the FILD scintillator in the vessel. We calculated orbits of escaping ^{3}He-ions with pitch-angle $\theta = 64°$ back-in-time from the FILD scintillator plate (figure 11). The orbits with gyro-radii $\rho_{gyr} = 10$ cm and 13 cm have the turning points at 2.90 m and 2.85 m consequently, i.e. they are in the vicinity of the MC layer, the region where an intense wave damping occurs by ^{3}He-ions.

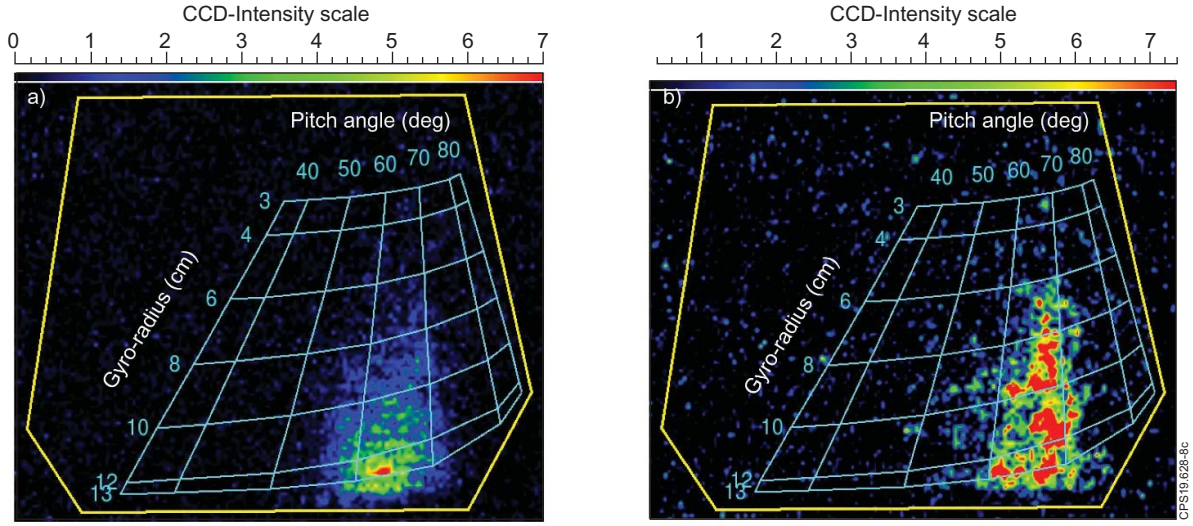

Figure 8. Footprints of losses in the discharge #91304 recorded with CCD camera: (*a*) in the period 9.94–10.34 s during the TAEs; (*b*) during the monster sawtooth crash 10.39–10.41 s.

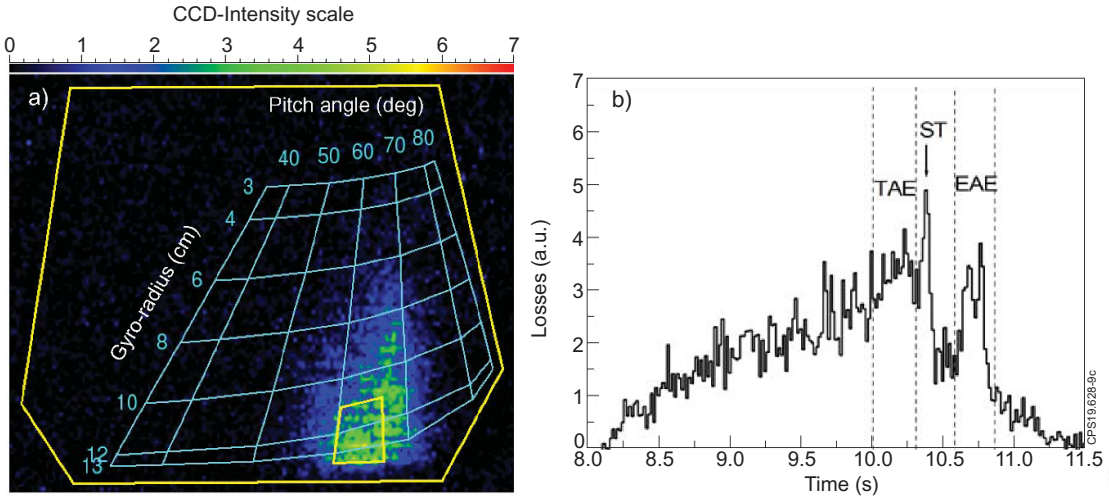

Figure 9. (*a*) Footprint of losses in the discharge #91304 recorded with CCD camera in the period 9.94–10.79 s during the TAEs, the monster sawtooth crash and EAEs; the yellow line shows the area used for making a wave form presented in (*b*): waveform of losses related to the scintillator areas designated in (*a*), which show a strong correlation with appearance of the TAE and EAE modes in the discharge.

3. Results of MHD analysis

In these experiments core localized TAEs with frequency $f_{\mathrm{TAE}} \approx 280$ kHz were observed. Following the phase with excitation of TAEs, strong EAEs at higher frequencies $f_{\mathrm{EAE}} \approx 550$–580 kHz with mode numbers $n = 1, 3, 5$ were seen. The high frequency modes indicate that the MeV range ^{3}He-ions in the plasma are interacting with the modes via $\omega = n\omega_\phi - p\omega_\theta$ resonance (here ω, n are the frequency and toroidal mode number of AE, ω_ϕ and ω^θ are toroidal precession drift and bounce frequencies of the energetic ions, and p is integer). This resonance condition for drift-precession is a standard result from the linear drift-kinetic theory [18]. Although any integer values of p equally satisfy the resonance condition, for trapped orbits with moderate bounce angle the strongest wave-particle energy transfer is expected for values of p close to $p = 0$ [19]. Calculations of ω_ϕ and ω_θ were performed for unperturbed ^{3}He-ion orbits with the HAGIS code [20]. HAGIS was used to solve for the first order guiding centre motion of test particles in the presence of the EFIT reconstruction of the equilibrium magnetic field. The test particles were assumed to arise from an on-axis ICRH resonance with $\Lambda \equiv \frac{\mu B_0}{E} = 1$. All possible orbits may be labelled with three invariants of motion: energy E, the parameter Λ, and the toroidal canonical momentum P_ϕ. For trapped orbits, the parallel velocity vanishes and the banana tip location along Z may be used as an invariant instead of P_ϕ. Resonance maps may then be produced by plotting $\log \sum_p \left(|n\omega_\phi - p\omega_\theta - \omega|\right)^{-|\alpha|}$ for values of p near zero, and where α is chosen to improve contrast in the figure depending on resolution.

The TAE resonance condition analysis shows (figure 12) that the mode with frequency and toroidal number $f = 280$ kHz, $n = 3$ could be excited by ^{3}He-ions in the

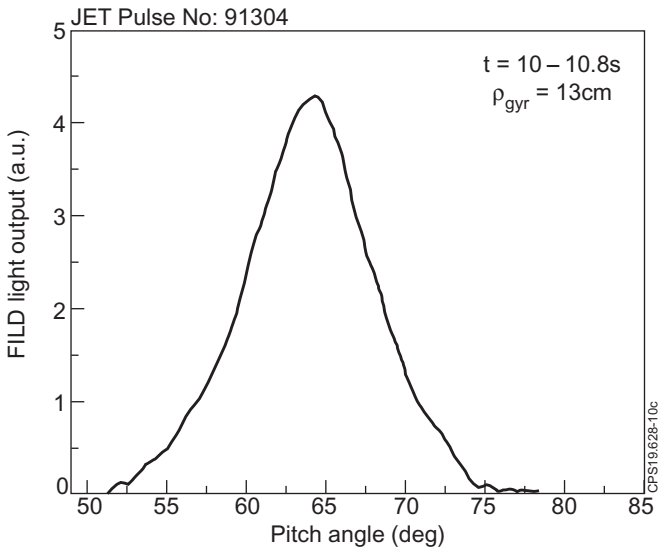

Figure 10. The pitch-angle distribution of lost ions with $\rho_{\rm gyr} = 13$ cm obtained from the FILD footprint data presented in figure 9(*a*)

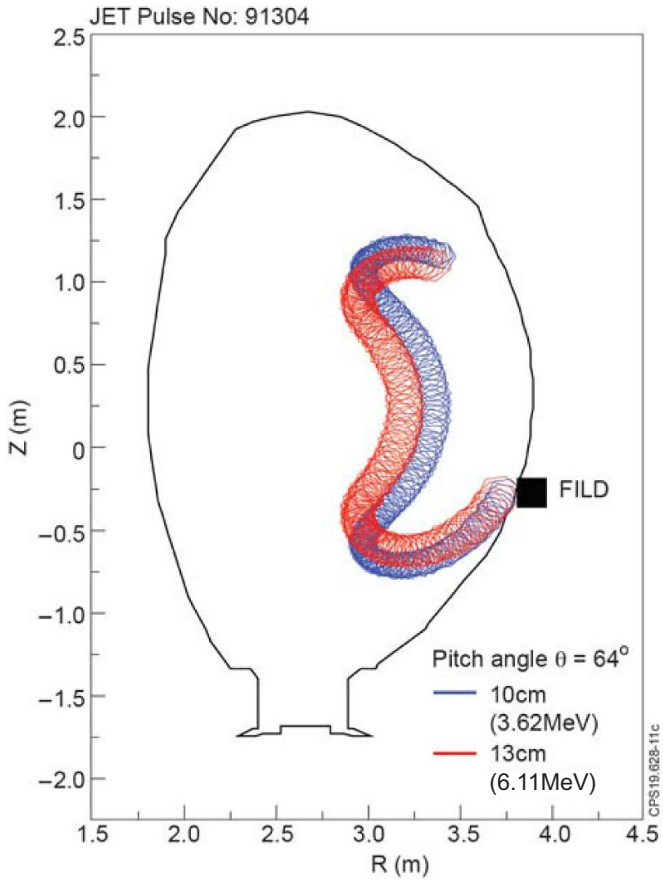

Figure 11. Orbits of ^{3}He-ions with gyro-radii 10 and 13 cm and pitch-angle 64° calculated back-in-time from the FILD scintillator plate; these parameters are related to the footprint presented in figure 9(*a*)

energy range 3–4 MeV. In the case of EAEs $n = 3$, $p = [-2, -1, 0]$, the strongest wave particle interaction is expected ion energies of $E_{3\rm He} \approx 6$ MeV to excite the modes with 560 kHz (figure 13(*a*)). However, for EAEs with $n = 1$, the resonance map shows that the modes with 560 kHz are much more difficult to excite and only $p = -2$ appearing at these energies (figure 13(*b*)).

During the studied discharge, we did not measure the q-profile with MSE diagnostics. Nevertheless, for the MHD analysis, the EFIT equilibrium has been used, which was reprocessed with pressure constraint, giving good agreement with MHD spectroscopy on the ECE diagnostic data, i.e. MHD markers $q = 1.5$ at 3.37 ± 0.05 m; a weak $n = 3$ mode, which gave us the position of $q = 4/3$ ($q \approx 1.33$ at 3.32 ± 0.05 m); sawteeth indicated that $q = 1$ at 3.15 ± 0.05 m. Figure 14 depicts the q-profile provided by the pressure-constrained EFIT.

The linear MHD code MISHKA [20] identified a core localised $n = 3$ EAE with frequency 539 kHz, giving agreement within ~5% of measured values, however the ideal MHD EAE solution was obtained only for the radial positions inside the $q \approx 1.33$ surface, where the EAE gap in the Alfvén continuum closes. The calculated EAE electrostatic potential is presented in figure 15 together with orbits of lost ^{3}He-ions with gyro-radii 10 cm (*a*) and 13 cm (*b*) that was calculated back-in-time from the FILD scintillator plate (figure 11). The loss orbits with $\rho_{\rm gyr} \approx 10$–13 cm are crossing inside $R = 3.3$ m and therefore interact with the ideal MHD EAE. Non-ideal effects are required to resolve mode beyond $R = 3.3$ m. It is important to note that calculated orbits are related to ions with the pitch-angle $\theta = 64°$ that have the bounce reflections in the region of the MC layer. Hence, the MHD analysis gives the mode locations, which are consistent with the experimental observations.

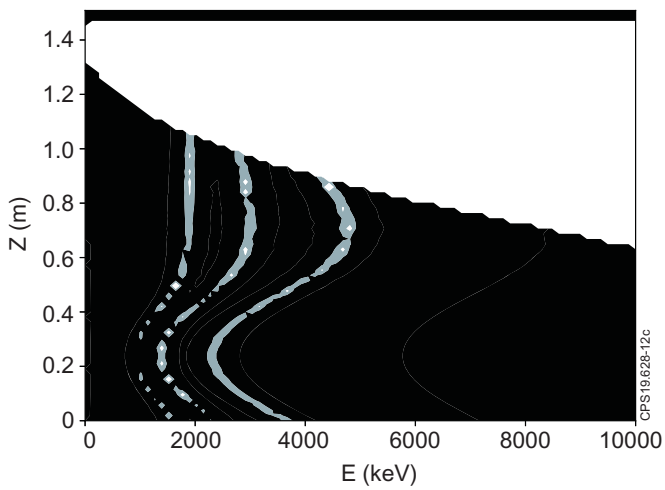

Figure 12. A resonance map $\omega = n\omega_\phi - p\omega_\theta$ for TAEs with frequency $f = 280$ kHz and toroidal number $n = 3$.

4. Summary and conclusions

The EAE and TAE instabilities were observed in hydrogen-rich, $n_{\rm H}/(n_{\rm H} + n_{\rm D})$ ~ 70%–90%, JET discharge #91304 of the D-(^{3}He)-H three-ion ICRH scenario, which has demonstrated

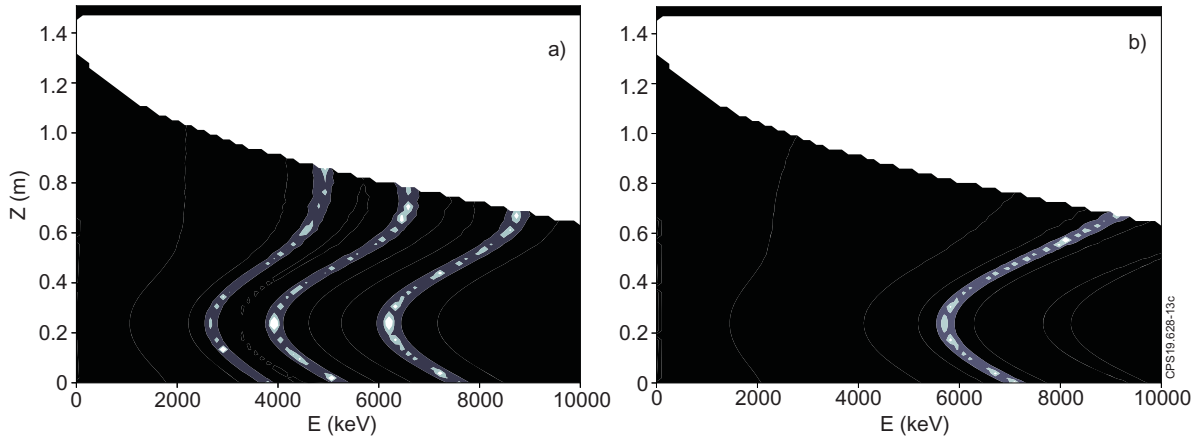

Figure 13. A resonance map $\omega = n\omega_\phi - p\omega_\theta$ for EAEs with frequency $f = 560$ kHz and toroidal numbers: (*a*) $n = 3$ and; (*b*) $n = 1$.

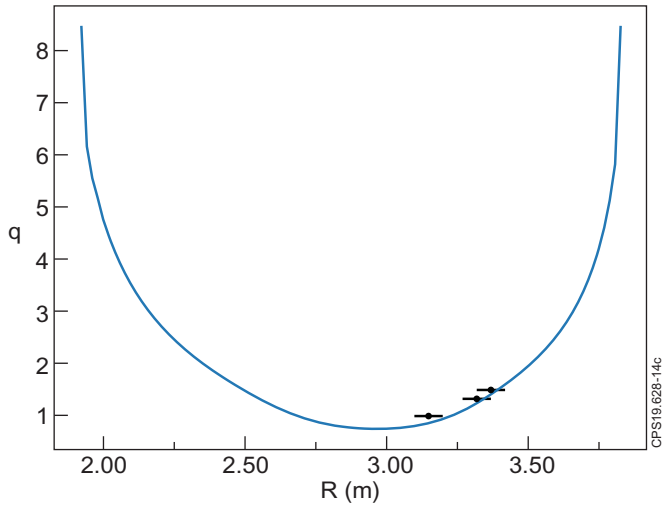

Figure 14. q-profile used for MHD analysis and MHD markers (black dots).

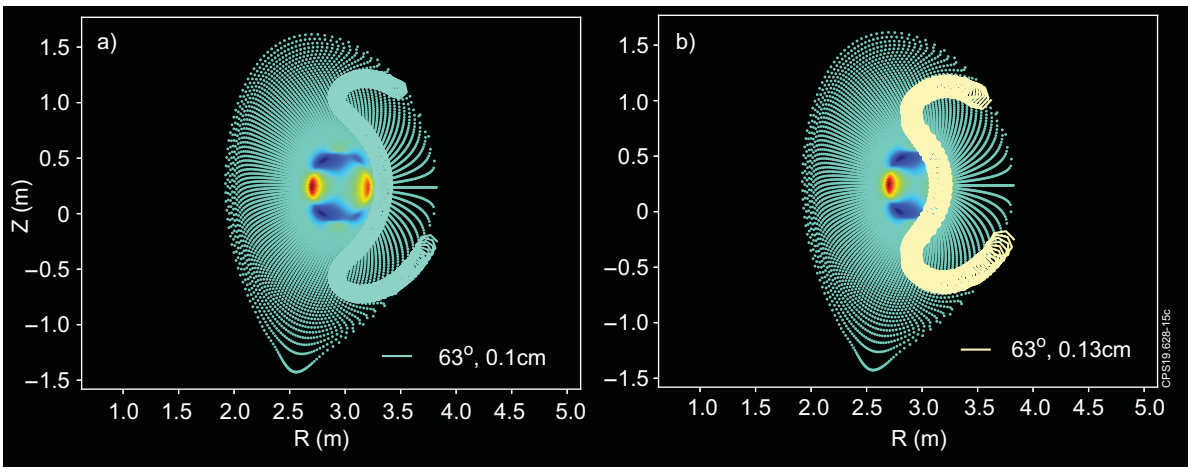

Figure 15. The linear mode electrostatic potential shows location of the EAE modes. Orbits of ^{3}He-ions with gyro-radii 10 cm (*a*) and 13 cm (*b*) and pitch-angle 64° calculated back-in-time from the FILD scintillator plate (see figure 11).

a strong absorption of radio frequency waves at very low concentrations (<1%) of the resonant ^{3}He-ions. In the experiments, core localized TAEs with a frequency $f_{\mathrm{TAE}} \approx 280$ kHz were observed. Following the phase with TAEs excitation, EAEs at higher frequencies $f_{\mathrm{EAE}} \approx 550$–580 kHz with mode numbers $n = 1, 3, 5$ were seen. These high frequency modes indicate that a MeV range population of trapped energetic ions was present in the plasma interacting with the modes via $\omega = n\omega_\phi - p\omega_\theta$ resonance. The experimental evidence of the existence in the plasma of the MeV-energy ^{3}He-ions, which are able to excite the AEs, is provided by neutron and gamma-ray diagnostics as well as fast ion loss measurements. It was found that the anomalous *DD* neutron rate in the ICRF-only heated plasma was provided by a population of energetic deuterons formed via knock-on effect: $D(^3\mathrm{He},\ ^3\mathrm{He})D_{\mathrm{knock-on}} \Rightarrow D\,(D_{\mathrm{knock-on}},\ n)\,^3\mathrm{He}$. Gamma-ray diagnostics showed that some neutrons are also generated in the nuclear reaction $^9\mathrm{Be}(^3\mathrm{He},\ n)^{11}\mathrm{C}$, which takes place with ^{3}He-ions in the MeV-range. The fast ion loss detector indicated that the MeV ^{3}He-ion losses related to the core localized TAEs ended with a spike associated with a monster sawtooth, after which the losses correlated with the EAE modes were observed. The analysis of FILD data indicates that the lost ^{3}He-ion energies exceed 2 MeV. The MHD analysis results are consistent with the experimental data showing that the MeV ^{3}He ions are resonant, when interacting with TAE and EAE modes.

The JET shot #91304 analysed here is unique as it is a discharge with effective ICRF-only plasma heating, where the MeV ^{3}He ions excite EAEs. However, there are discharges with excitation of TAEs by ^{3}He ions that we have observed [2].

The experiments described in this paper are mimicking the conditions representative for ITER plasmas and contribute to both the understanding of fast-ion interaction with MHD modes and the understanding of the impact of energetic ions on the plasma turbulence, in particular, the impact of alphas in ITER [22].

Acknowledgments

This work has been carried out within the framework of the EUROfusion Consortium and has received funding from the Euratom research and training programme 2014–2018 and 2019–2020 under Grant Agreement No. 633053 and from the RCUK Energy Programme (Grant No. EP/T012250/1). To obtain further information on the data and models underlying this paper please contact PublicationsManager@ukaea.uk. The views and opinions expressed herein do not necessarily reflect those of the European Commission.

ORCID iDs

M. Nocente https://orcid.org/0000-0003-0170-5275
M.F.F. Nave https://orcid.org/0000-0003-2078-6584

References

[1] Kazakov Y.O., Van Eester D., Dumont R. and Ongena J. 2015 *Nucl. Fusion* **55** 032001
[2] Kazakov Y.O. *et al* 2017 *Nat. Phys.* **13** 973–8
[3] Mantsinen M. *et al* 2019 Modelling of three-ion ICRF schemes with PION *46th EPS Conference on Plasma Physics* (Milan, Italy, 8-12 July 2019) O5.102 (http://ocs.ciemat.es/EPS2019ABS/pdf/O5.102.pdf)
[4] Kiptily V.G., Cecil F.E. and Medley S.S. 2006 *Plasma Phys. Control. Fusion* **48** R59–R82
[5] Nocente M. *et al* 2013 *IEEE Trans. Nucl. Sci.* **60** 1408–15
[6] Syme D.B. *et al* 2014 *Fusion Eng. Des.* **89** 2766–75
[7] Darrow D. *et al* 2006 *Rev. Sci. Instrum.* **77** 10E701
[8] Shevelev A.E. *et al* 2013 *Nucl. Fusion* **53** 123004
[9] *A General Monte Carlo N-Particle* (*MCNP*) *Transport Code* (https://mcnp.lanl.gov/)
[10] Eriksson L.G. *et al* 1993 *Nucl. Fusion* **33** 1037
[11] Nocente M. *et al* 2011 *Nucl. Fusion* **51** 063011
[12] Gatu Johnson M. *et al* 2010 *Nucl. Fusion* **50** 045005
[13] Wesson J.A. 1990 *Nucl. Fusion* **30** 2545
[14] Porcelli F. 1991 *Phys. Rev. Lett.* **66** 425
[15] Kolesnichenko Y.I. and Yakovenko Y.V. 1992 *Phys. Scr.* **45** 133
[16] Ottaviani M. *et al* 2004 *Plasma Phys. Control. Fusion* **46** B201
[17] Bosch H.S. and Hale G.M. 1992 *Nucl. Fusion* **32** 611–31
[18] Fredrickson E., Chen L. and White R. 2003 *Nucl. Fusion* **43** 1258–64
[19] Pinches S.D. *et al* 1998 *Comput. Phys. Commun.* **111** 133–49
[20] Mikhailovskii A.B. *et al* 1997 *Plasma Phys. Rep.* **23** 844–57
[21] Garcia J. *et al* 2018 *Phys. Plasmas* **25** 055902
[22] Porcelli F., Stankiewicz R. and Kerner W. 1994 *Phys. Plasmas* **1** 470